International Journal of Heat and Mass Transfer 87 (2015) 151–160

Contents lists available at ScienceDirect

International Journal of Heat and Mass Transfer

journal homepage: www.elsevier.com/locate/ijhmt

Velocity dependent Maxwell boundary conditions in DSMC

Alireza Mohammadzadeh *, Henning Struchtrup

University of Victoria, Victoria, B.C., Canada

ARTICLE INFO

Article history:
Received 30 September 2014
Received in revised form 3 March 2015
Accepted 13 March 2015

Keywords:
DSMC
Thermal transpiration
Thermal stress
Gas–surface interaction
Velocity dependent boundary conditions

ABSTRACT

Recently Struchtrup (2013) proposed an extension to the original Maxwell boundary conditions for the Boltzmann equation which introduces velocity dependent accommodation coefficients. These boundary conditions are implemented into the direct simulation Monte Carlo (DSMC) method. The effect of the velocity dependent Maxwell (VDM) boundary conditions on thermal transpiration phenomena is studied for two-dimensional micro-cavities. Variation of the three microscopic parameters provided by the VDM boundary condition yields changes in slip velocity, temperature jump and the thermal transpiration effect. The results indicate that the strength of thermal transpiration can change and, depending on the values of the coefficients, the rarefied flow can be driven from warmer toward colder regions.

1. Introduction

The interactions between gas particles and a solid surface are complex. It is unlikely that a general mathematical model be developed that can adequately describe the gas–surface interactions for different combinations of gases and surfaces at all conditions. However, by using microscopic simulation methods, such as direct simulation Monte Carlo (DSMC) [1] and molecular dynamics (MD) [2], better understanding of the interaction can be obtained. This knowledge helps in developing phenomenological models which can provide better fit to the experimental data.

Experiments with molecular beams show that the beam is scattered into a plume-like structure around the line of specular reflection [3,4]. The structure of the reflected beam becomes particularly important when scattered particles are free to move for a long distance inside the bulk gas. The Knudsen number, Kn, is defined as the ratio between the mean free path of the gas particles and the flow characteristic length scale, $Kn = \frac{\lambda}{L}$. Special attention should be given to the reflection kernel when the Knudsen number becomes large.

This plume-like structure is described and captured by the Cercignani–Lampis (CL) model [5,6], where the shape of the reflection plume strongly depends on the values of the normal and tangential accommodation coefficients, α_n and α_t. In this model, the collision outcome depends on the velocity of impacting particle with the surface. Although the CL model can be fitted to slip velocity and temperature jump, it does not provide sufficient flexibility to be fitted to the data for thermal transpiration coefficient [7].

For moderate Knudsen numbers, i.e., in the transition flow regime, the particles reflected from the surface travel a rather short distance before their first inter-molecular collision. In this regime the exact shape of the reflection plume is not required to express boundary conditions, but an appropriate approximation can deliver the chemistry of gas–surface interaction. This provides room for a simpler model than CL, which can be fitted to the thermal transpiration coefficient. The original Maxwell accommodation model [8], due to its simplicity, cannot predict different accommodation coefficients for the slip velocity and temperature jump.

Epstein [9] considered the effect of impact velocity on the reflection kernel, and proposed an extension to the Maxwell model. In this model the degree of thermal accommodation is determined based on the impact energy of the colliding particle.

Recently, Struchtrup [10] added the isotropic scattering kernel to the Maxwell's boundary condition to also account for nearly adiabatic surface with friction [11]. Also this model, by considering the impact velocity of the particles, allows to incorporate velocity dependent accommodation coefficients into the microscopic description. In the velocity dependent Maxwell (VDM) boundary condition, a particle colliding with the surface is either thermalized, specularly reflected, or scattered in an arbitrary direction, where the probabilities for the different processes depend on the impact velocity. The model provides wide flexibility for the choice of the velocity dependent accommodation coefficients. A particular model was suggested in Ref. [10], based on the assumption that the gas–wall interaction can be described as a thermally activated

* Corresponding author.
E-mail address: alirezam@uvic.ca (A. Mohammadzadeh).

http://dx.doi.org/10.1016/j.ijheatmasstransfer.2015.03.045
0017-9310/

process, where particles with higher velocities are more likely to be specularly reflected or isotropically scattered from the surface, while particles with smaller velocity are more likely to be thermalized. The corresponding macroscopic boundary conditions for slip velocity and temperature jump were obtained from the first order Chapman–Enskog expansion.

Thermally-driven flows inside a two-dimensional enclosure have been studied in the literature [12,13]. Vargas et al. [13] examined the effect of Knudsen number, surface temperature gradient and the geometry aspect ratio on the flow formation inside a micro cavity. They observed that the interplay between thermal transpiration and the viscous stresses in the boundary determines the direction of tangential velocity close to the wall. They also reported that close to the continuum regime thermal transpiration dominates, and the gas flows from colder to warmer regions.

The importance of boundary conditions in the thermal-driven flows has also attracted the attention of other researchers [14,15]. Cai [14] used the Maxwell boundary condition to study the flow formation inside a cavity subjected to a temperature profile on the wall. He considered two cases of continuum and free molecular regimes to see the effect of Knudsen number on the rarefied flow. Kosuge et al. [16] used the Maxwell and the CL model to study the steady flow between parallel plates with sinusoidal temperature distribution at large Knudsen numbers. They demonstrated that considering the CL model leads to a steady flow between the plates, whereas for the Maxwell-type model the gas remains at rest.

In the current study, the velocity vector for particles reflecting from the surface is derived, and the required steps to implement the VDM boundary conditions into a DSMC solver are presented. To study the effects of thermal transpiration, rarefied flows inside a two-dimensional thermal cavity with temperature gradient along the surface are considered. The effects of the three independent coefficients incorporated in the VDM boundary conditions on the vortex formation, and strengthening or weakening of the rarefaction effects are studied. The results indicate that, in contrast to the CL model, the VDM boundary condition provides opportunity for fitting to experimental data for transpiration flow.

The remainder of the paper is organized as follows. A short description of the DSMC method employed in this study is presented in Section 2. The general reflection kernel for the VDM boundary conditions is rephrased in Section 3.1; then the reflecting velocity for use in the DSMC method is obtained and presented. The geometry considered in this study is presented in Section 4.1, and the boundary conditions are tested in a micro cavity to ensure the persistency of the Maxwell distribution function. Afterward, the flow formation inside a micro cavity with temperature gradient is studied in Section 4.2. A brief description of the thermal transpiration flow is presented, and the possibility of inverse transpiration flow is discussed in Section 4.3. We shortly mention the hydrodynamic boundary equations for the VDM model, and use the Grad equations to explain the flow formation. The DSMC solution for the thermal cavity in larger rarefaction regime is presented in Section 4.4. The paper ends with our conclusions in Section 5.

2. DSMC method

The DSMC method is a numerical tool to solve the Boltzmann equation by using the statistical simulation of molecular processes based on the kinetic theory of dilute gases [1]. In this method, many independent simulating particles are used to model gaseous flows, where each particle represents a large number of real gas molecules. For the current study, we modified our DSMC solver [17–19,12,11] by implementing the VDM boundary condition. In this code, the selection of collision pairs is based on the no-time-counter (NTC) method, therefore the computational time is proportional to the number of the simulating particles [1]. The fluid is argon as a Maxwell molecule with $m = 6.63 \times 10^{-26}$ kg and the reference viscosity of $\mu_0 = 1.9549 \times 10^{-5}$ Pa.s. The Knudsen number is defined as [20]

$$Kn = \frac{\mu_0}{\rho_0 \sqrt{RT_0} L}. \tag{1}$$

Here, ρ_0 is the reference density, and L indicates the characteristic length of the flow. The DSMC simulation starts with 32 particles located in each cell. As the flow reaches the steady state, the molecular properties are sampled over a large period of time to reduce the statistical scattering. In addition, a filtering post processor is used to minimize the scattering in the thermodynamic properties. In this filtering, the sampled macroscopic properties, F, in cell N are averaged over a pattern of its neighboring cells [17]

$$\tilde{F}_{(N)} = \frac{F_N + \sum_{I=1}^{I=N_n} F_I}{N_n + 1}.$$

3. VDM boundary conditions

3.1. Reflection kernel

The reflection kernel for the generalized Maxwell model can be written as a superposition of diffuse reflection, specular reflection, and isotropic scattering [10],

$$P(\mathbf{c}' \to \mathbf{c}) = \Theta(c') \frac{|c_n| f_0 \Theta(c)}{\int_{c_n>0} |c_n| f_0 \Theta(c) d\mathbf{c}} + (1 - \Theta(c')) \times \left[\gamma \delta(c'_k - c_k + 2 n_j c_j n_k) + (1-\gamma) \frac{1}{\pi} \frac{|c_n|}{c'^3} \delta(c' - c) \right]. \tag{2}$$

Here, c'_k and c_k denote velocities of incoming and outgoing particles, respectively, c' and c are the respective absolute values, and $c_n = c_k n_k$ is the contribution normal to the wall. The velocity dependent accommodation coefficient $\Theta(c')$ is the probability that an incoming particle will be diffusively reflected, and the coefficient γ is introduced so that $\gamma(1 - \Theta(c'))$ is the probability that a particle will be specularly reflected.

Many meaningful models for the coefficients $\Theta(c)$ and γ can be developed [9]. In the following we use the model suggested in Ref. 10, where $\gamma = const$, and thermalization is assumed as a thermally activated process,

$$\Theta(c') = \Theta_0 \exp\left(\frac{\varepsilon - \alpha \frac{m}{2} c'^2}{k T_W} \right). \tag{3}$$

Here, the dimensionless coefficient α is a measure for the strength of the activation, where $\alpha = 0$ as a case without activation, corresponds to the original Maxwell model with fully diffusive walls. Moreover, ϵ considers the effect of energy bounce on the reflected particle, and Θ_0 is a constant depending on the wall structure. Note that these coefficients can be varied so that the results fit to the experimental data. In the following we assume that $\Theta_0 = 1$ and $\epsilon = 0$ unless otherwise mentioned. In Eq. (2), $f_0 = 2\beta\sqrt{\pi} f_M / \rho$ is the reduced Maxwell distribution in the rest frame, which with the above notation can be written as, with $\beta = \sqrt{\frac{m}{2kT}}$,

$$f_0 = \frac{2}{\pi} \beta^4 \exp\left(-\beta^2 c^2\right).$$

The probability function, Eq. (3), varies between 0 and 1, and depends on the velocity c' of the particle colliding with the surface. To determine whether the particle is diffusively reflected or

scattered, a random number, $R_1 \in [0,1]$ is drawn, such that the particle undergoes a diffuse reflection if $R_1 < \Theta(c')$. If, however, $R_1 > \Theta(c')$, a second random number $R_2 \in [0,1]$ is drawn, and the scattering is specular for $R_2 < \gamma$, and isotropic for $R_2 > \gamma$. For each of these cases, the reflection kernel is selected according to the following rules:

3.2. Diffusive reflection, $R_1 < \Theta(c')$

The first term of Eq. (2) determines the velocity of a diffusively reflecting particle, i.e., the reflection kernel is

$$P_D(\mathbf{c}' \to \mathbf{c}) = \frac{|c_n| f_0 \Theta(c)}{\int_{c_n>0} |c_n| f_0 \Theta(c) d\mathbf{c}}.$$

To proceed, we consider the particle velocity in cylindrical coordinates, so that $\mathbf{c} \to \{c_n, c_r, \theta\}$ and $d\mathbf{c} = c_r dc_n dc_r d\theta$. For the implementation into DSMC we need the cumulative probability that a particle leaves with a velocity below $\{V_n, V_r, \Omega\}$, defined as

$$F_n F_r F_\Omega = \int_0^{V_n} \int_0^{V_r} \int_0^{\Omega} P_D(\mathbf{c}' \to \mathbf{c}) c_r dc_n dc_r d\theta. \tag{4}$$

Here, F_n, F_r and F_Ω are the cumulative probabilities for the velocity vector in cylindrical coordinates. Making f_0 and $\Theta(c)$ explicit, and performing all integrations, we find at first

$$F_n F_r F_\Omega = \frac{2\int_0^{V_n} \beta^2 c_n \exp\left(-(1+\alpha)\beta^2 c_n^2\right) dc_n}{2\int_0^{\infty} \beta^2 c_n \exp\left(-(1+\alpha)\beta^2 c_n^2\right) dc_n} \times \frac{2\int_0^{V_r} \beta^2 c_r \exp\left(-(1+\alpha)\beta^2 c_r^2\right) dc_r}{2\int_0^{\infty} \beta^2 c_r \exp\left(-(1+\alpha)\beta^2 c_r^2\right) dc_r} \frac{\int_0^{\Omega} \frac{d\theta}{2\pi}}{\int_0^{2\pi} \frac{d\theta}{2\pi}}. \tag{5}$$

The above integrals can be calculated analytically, and Eq. (4) simplifies to

$$F_n = 1 - \exp\left(-(1+\alpha)\beta^2 V_n^2\right),$$
$$F_r = 1 - \exp\left(-(1+\alpha)\beta^2 V_r^2\right),$$
$$F_\Omega = \frac{\Omega}{2\pi}.$$

Solving the above equations for the three upper limits of integral gives

$$V_n = \frac{1}{\sqrt{1+\alpha}} \frac{1}{\beta} \sqrt{-\ln(1-F_n)},$$
$$V_r = \frac{1}{\sqrt{1+\alpha}} \frac{1}{\beta} \sqrt{-\ln(1-F_r)},$$
$$\Omega = 2\pi F_\Omega.$$

By converting back to the Cartesian coordinates for a surface with normal in y-direction, the reflecting velocities are obtained as

$$c_x = \frac{1}{\sqrt{1+\alpha}} \frac{1}{\beta} \sqrt{-\ln(1-F_r)} \cos(2\pi F_\Omega),$$
$$c_y = \frac{1}{\sqrt{1+\alpha}} \frac{1}{\beta} \sqrt{-\ln(1-F_n)}, \tag{6}$$
$$c_z = \frac{1}{\sqrt{1+\alpha}} \frac{1}{\beta} \sqrt{-\ln(1-F_r)} \sin(2\pi F_\Omega).$$

The cumulative probabilities are uniformly distributed in $[0,1]$. The velocity of the thermalized particle is determined by drawing three random numbers for $\{F_n, F_r, F_\Omega\}$, and computing the velocity from the above.

Compared to the corresponding expressions for the standard Maxwell boundary conditions, the VDM boundary condition contains the factor $\frac{1}{\sqrt{1+\alpha}}$ that is due to the velocity dependence of the accommodation coefficient $\Theta(c')$. Assuming $\alpha = 0$ gives the conventional Maxwell boundary conditions for the diffusive wall [1].

3.3. Specular reflection, $R_1 > \Theta(c')$ and $R_2 < \gamma$

A particle is specularly reflected if $R_1 > \Theta(c')$ and $R_2 < \gamma$. The reflection kernel

$$P_{Sp}(\mathbf{c}' \to \mathbf{c}) = \delta\left(c_k' - c_k + 2n_j c_j n_k\right),$$

describes the deterministic specular reflection of the particle, with the after-collision velocity

$$c_x = c_x', \quad c_y = -c_y', \quad c_z = c_z'.$$

3.4. Isotropic scattering, $R_1 > \Theta(c')$ and $R_2 > \gamma$

Isotropic scattering occurs when $R_1 < \Theta(c')$ and $R_2 > \gamma$, and the corresponding reflection kernel is

$$P_{Sc}(\mathbf{c}' \to \mathbf{c}) = \frac{1}{\pi} \frac{|c_n|}{c'^3} \delta(c' - c).$$

By using spherical coordinates, $\{c, \theta, \phi\}$ we can write

$$P(\mathbf{c}' \to \mathbf{c}) d\mathbf{c} = \frac{1}{\pi c'^3} c \cos\phi \delta(c' - c) c^2 dc \sin\phi d\phi d\theta$$
$$= [\delta(c' - c) dc] \left[\frac{1}{2\pi} d\theta\right] [2\cos\phi \sin\phi d\phi].$$

The delta function indicates that the absolute velocity of the leaving particle is deterministic, $c = c'$. However, the direction of the leaving particle is subjected to the process of random scattering, and as before we consider the cumulative probabilities

$$F_\theta = \int_0^{\Theta} \frac{1}{2\pi} d\theta, \quad F_\phi = \int_0^{\Phi} 2\cos(\phi)\sin(\phi) d\phi,$$

The integrals for the cumulative probabilities F_θ, F_ϕ can be solved analytically to give

$$\Theta = 2\pi F_\theta, \quad \Phi = \arcsin(\sqrt{F_\phi}) \tag{7}$$

By converting back the velocity components to the Cartesian coordinates, and noting that $\cos(\arcsin(x)) = \sqrt{1-x^2}$, the velocity of the scattered particle is

$$c_x = c' \sqrt{F_\phi} \cos(2\pi F_\theta),$$
$$c_y = c' \sqrt{1 - F_\phi}, \tag{8}$$
$$c_z = c' \sqrt{F_\phi} \sin(2\pi F_\theta).$$

The cumulative probabilities are uniformly distributed in $[0,1]$. The velocity of the isotropically scattered particle is determined by drawing two random numbers for $\{F_\phi, F_\theta\}$, and computing the velocity from the above.

4. Results and discussion

4.1. Persistency of Maxwell distribution in micro-cavity

We consider a square micro-cavity as depicted in Fig. 1a. The temperature of the wall in the micro-cavity, T, varies along the x and y-directions as indicated. We are interested in transpiration flow, where the driving force for the flow in the cavity is the temperature gradient along the surfaces.

In the DSMC method particles are initially distributed according to the Maxwellian distribution function [1]. In this section we ensure that in a system without perturbation the Maxwell distribution persists, when particles collide with the VDM boundary

condition and reflect back to the flow. For this test, the rarefied flow in the micro-cavity is left to itself, and the microscopic velocity distribution function as well as the macroscopic velocity profile are obtained. The wall temperatures in the micro-cavity are prescribed as

$$T_B = T_L = T_T = T_R = 300\ \mathrm{K}.$$

The coefficients for the VDM boundary conditions assumed in this test are

$$\varepsilon = 0, \quad \alpha = 0.5, \quad \gamma = 0.7 \quad \Theta_0 = 1.$$

Fig. 1b demonstrates the normalized horizontal velocity distribution function for a computational cell in the top left corner of the cavity. It is observed that the distribution obtained from the DSMC simulation agrees with the local Maxwellian distribution, obtained from the local values for density, velocity and temperature. The horizontal macroscopic velocity distribution inside the cavity in Fig. 1c shows that the persistency of the Maxwellian distribution is well guaranteed by the implementation of this new set of boundary conditions.

4.2. Micro-cavity

The flow formation inside the micro-cavity is considered for the case where the temperature of the side walls varies linearly, specifically we set

$$T_B = 600\ \mathrm{K} \quad T_T = 300\ \mathrm{K} \quad T_L(y) = T_R(y) = T_B\left(1 + \frac{y}{L}\right).$$

Fig. 2 shows the effect of the coefficients Θ_0, α and γ on the velocity streamlines and the temperature distribution inside the cavity.

The left column in Fig. 2 shows the DSMC results when the reflection kernel *does not* depend on the velocity of impacting particle, $\alpha = 0$. The right column, on the other hand, shows the flow formation when dependency of the reflection on the impact velocity is considered, $\alpha \neq 0$.

Starting from the fully diffusive surface, Fig. 2a we observe that the tangential component of the velocity vector close to the vertical wall is downward: thermal transpiration pushes the rarefied flow towards the bottom (i.e., the warmer) side of the cavity.

Considering the impact velocity on the reflection kernel using the VDM boundary condition, decreases the magnitude of the vertical velocity close to the vertical walls. As we increase α and γ, an additional vortex which drives the rarefied flow toward the upper (i.e., colder) side of the cavity appears (Fig. 2e and f). In other words, sufficiently large values of α and γ in the VDM boundary condition lead to a decreased strength of the thermal transpiration phenomenon, and the appearance of warm-to-cold vortices.

In order to confirm the effect of impact velocity on the formation of the secondary vortex, we performed the simulation when the reflection kernel does not depend on the impact velocity $\alpha = 0$, but contains diffusive, specular and isotropic scattering. In order to have a comparable setting we adjust Θ_0 such that it is the average probability for a diffusive reflection, defined as $\bar{\Theta} = \int_{c_n<0} \Theta(c) c_n f_M d\mathbf{c} / \int_{c_n<0} c_n f_M d\mathbf{c}$ which gives $\bar{\Theta} = (1+\alpha)^{-2}$. For comparison with the case for $\alpha = 0.2$, we hence chose $\Theta_0 = 0.7$, and perform the simulation for two values of γ. As depicted in Fig. 2b and c, the secondary vortex does not appear when the reflection kernel is independent of the impact velocity. This figure indicates that, in the case of VDM boundary condition, the dependency of the reflection kernel on the impact velocity is required to weaken/increase the strength of the thermal transpiration effect.

Smaller transpiration effects in the VDM boundary condition allows other non-equilibrium phenomena, such as thermal stresses, to play a more important role in determining the flow direction close to the surface. The reversed direction of velocity close to the surface also suggests the possibility of reversed transpiration flow, where the rarefied flow is driven from warm to cold; this will be discussed in greater detail in Section 4.3.

Comparing the temperature distributions inside the cavity shows that the VDM boundary condition leads to smaller temperature gradients inside the cavity. Since not all particles are forced to thermalize with the surface after collision, the wall information will not be completely transferred to the flow field, so that the temperature jump is larger, which leads to smaller maximum, and larger minimum temperature inside the cavity.

Fig. 3 shows the rarefied flow properties along the vertical line $\frac{X}{L} = 0.95$, which lies inside the Knudsen layer of the right wall. The VDM boundary condition allows some particles to reflect back to the flow without exchanging momentum, or energy, with the surface, which subsequently decreases the shear stress along the wall. It is also seen that the effect of changing γ on the tangential velocity is quite different for standard Maxwell and the VDM boundary condition. In the case of standard Maxwell boundary condition, the tangential velocity is not much dependent on γ. As α and γ increases, the shear stress and the vertical velocity become smaller in magnitude, see Fig. 3a and b, and the velocity changes sign when the small vortex close to the right wall appears. Fig. 3c shows

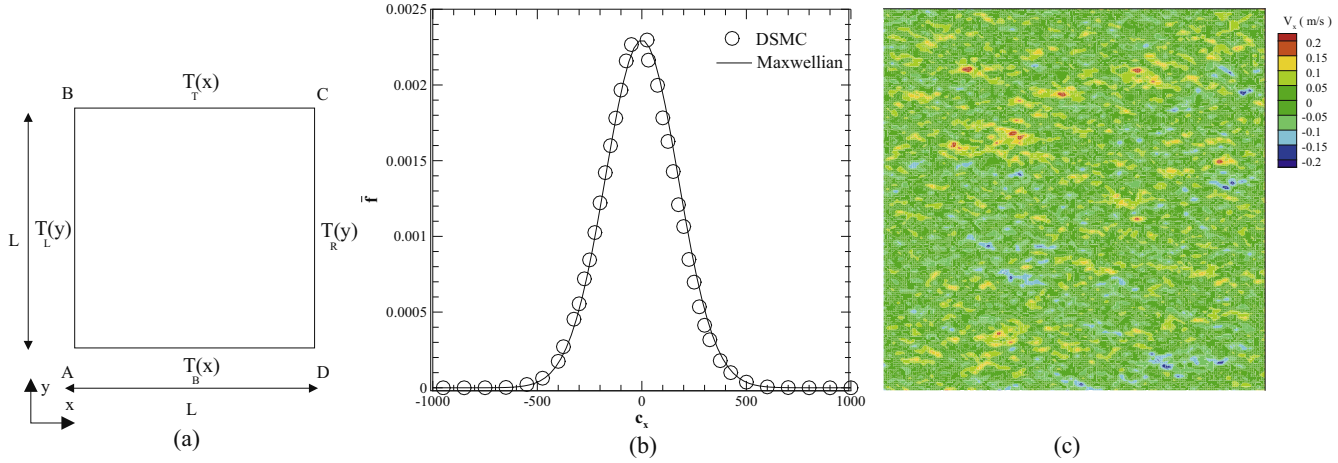

Fig. 1. Persistency of the Maxwell distribution in micro-cavity, (a) cavity geometry, (b) normalized microscopic horizontal velocity distribution function, (c) macroscopic horizontal velocity distribution in the micro-cavity.

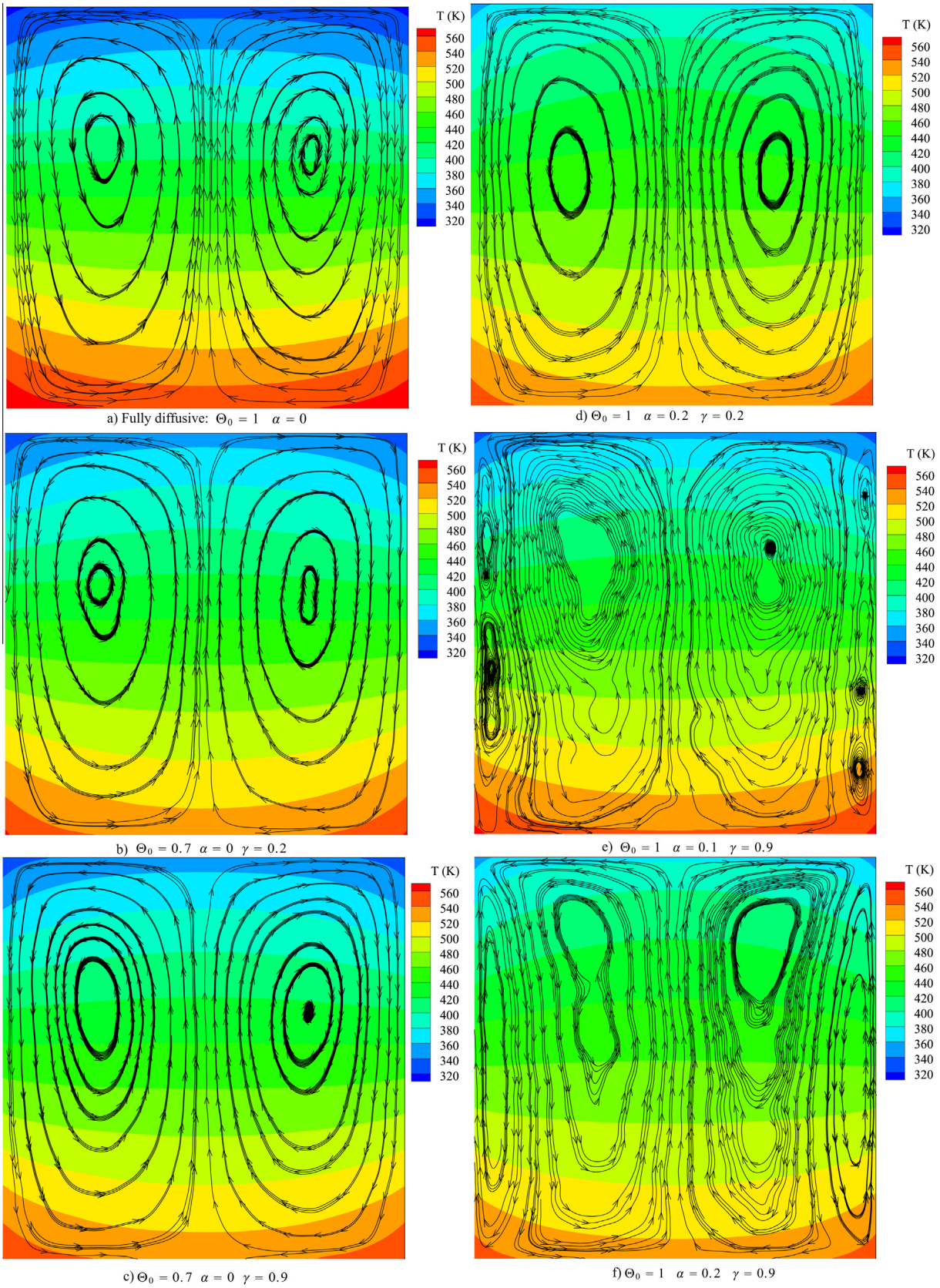

Fig. 2. Velocity streamlines overlaid on the temperature distribution, $Kn = 0.1,\ \varepsilon = 0$.

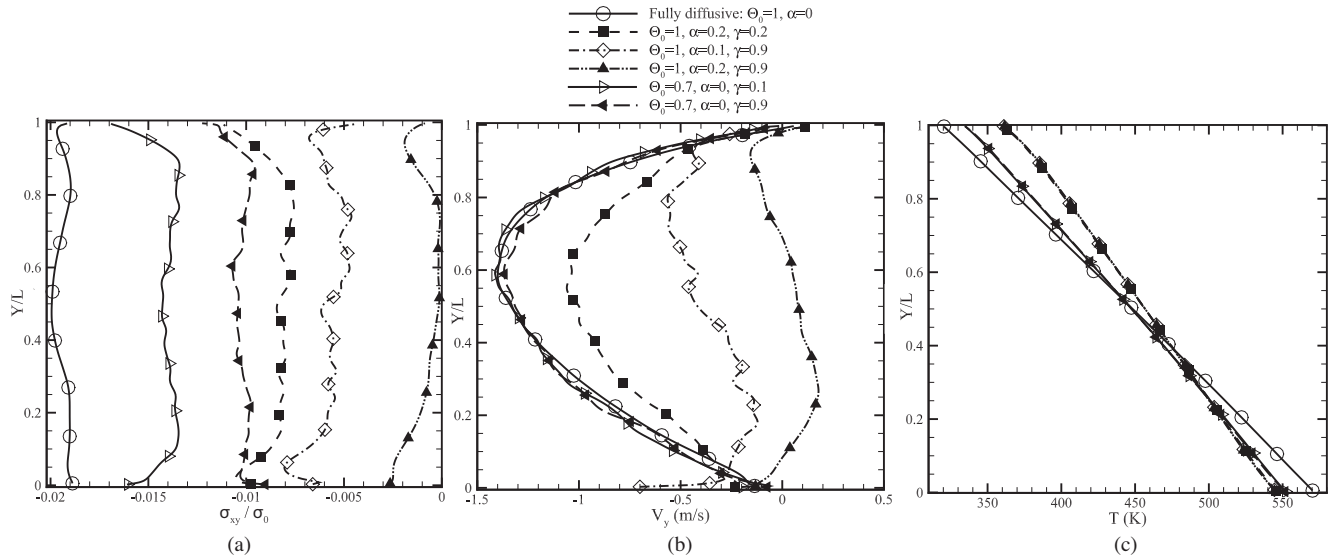

Fig. 3. The effect of Θ_0, α and γ coefficient on the flow properties along $\frac{X}{L} = 0.95$ for $Kn = 0.1$, $\varepsilon = 0$.

smaller gradient of temperature for the new reflection kernel, which appears to be unaffected by the coefficients in the VDM model.

4.3. Forward and inverted transpiration flow

Thermal transpiration takes place when two particles coming from the cold (smaller thermal velocity) and warm (higher thermal velocity) regions exchange momentum with the surface at the same location. Fig. 4 shows an schematic of the particle–surface interaction for the two types of boundary conditions.

The left figure shows the collisions for the classical Maxwell boundary model, where the accommodation is independent of impact velocity. Since the collision kernel is isotropic, the average reflection velocities for the particle colliding with the wall is perpendicular to the wall, as indicated by the dashed vectors. Therefore, in average, the complete tangential momentum of an incoming particle is transferred to the wall. Since the particle coming from the warmer region has a higher impact velocity, it can induce a greater force on the wall, so that the net force on the wall points toward the colder region, see F_W in Fig. 4a. As a reaction, the wall drives the rarefied flow toward the warmer region by imposing a shear force on the flow, F_G. Consequently, the gas moves in the direction of the wall temperature gradient.

In the VDM boundary condition, as shown in the right figure, a particle with higher velocity c' relative to the surface has a higher chance, $\gamma(1 - \Theta(c'))$, to be specularly reflected, which implies no exchange of tangential momentum. Accordingly, a larger number of slower particles–coming from the colder region–transmit their tangential momentum to the wall, compared to a smaller number of fast particles–coming from the warmer region. As α increases, larger number of particles with high impact velocity skip the thermalization process with the surface, and reflect back to the bulk without any momentum exchange. For relatively large values of α and γ, the colder particles will transfer more tangential momentum than the warmer particles, which results in a net force on the wall toward the warmer region. That is, the force F_W changes its sign as compared to the standard transpiration flow, see Fig. 4b. This leads to the movement of the gas relative to the wall, from warm to cold. It is also worth noting that the magnitude of shear force on flow, F_G, becomes smaller since less momentum is transferred due to more specular reflections.

While the above argument shows the theoretical possibility of inverted transpiration flow, it is not clear that the occurrence of the secondary vortices in the VDM model can actually be

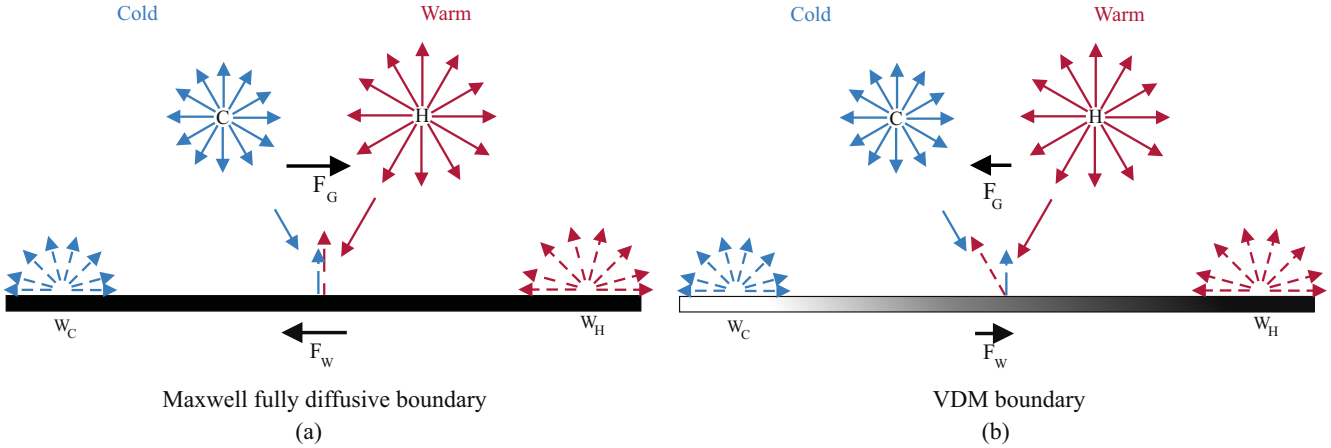

Fig. 4. Thermal transpiration effect over the conventional Maxwell and VDM boundary conditions.

attributed to this effect. In order to examine the transpiration phenomena on the microscopic level, we used DSMC results to compare the tangential momentum that particles exchange with the right wall of the micro-cavity. We keep the thermal configuration of the cavity as in Section 4.2, and define the tangential momentum exchange between a particle and the surface as

$$M_j = m\overline{(c_t' - c_t)}_j.$$

Here, c_t' and c_t are the tangential velocities before and after collision with the surface element j, and the overbar indicates the time average of the microscopic quantity. Particles with positive tangential impact velocity, $c_t' > 0$, come from a warmer region (they move upward), i.e., they have larger thermal velocity, and exchange the momentum M_j^H with the surface. Particles with negative tangential impact velocity, $c_t' < 0$ come from the colder region (they move downward) and exchange the momentum M_j^C with the surface. Fig. 5 shows the variation of exchanged momentum for the VDM boundary condition along the surface. The tangential momenta are non-dimensionalized with respect to $M^0 = m\sqrt{2\frac{k}{m}T_B}$.

As the coefficients α and γ increase, we observe a decrease in the exchanged momentum from both, colder and warmer particles. This result is in accordance with the reduction of shear stress inside the Knudsen layer in Fig. 3a. However, the decrease in the warmer momentum exchange, M_j^H is larger than the decrease in colder exchange M_j^C. For larger α and γ, the warmer particles have a higher chance to be specularly reflected, which implies that no tangential momentum is exchanged with the surface. The total momentum exchange, obtained from adding the two sources of tangential momentum, determines the direction of thermal transpiration force. It is observed that increasing the coefficients in the VDM boundary conditions can reduce the strength of the thermal transpiration effect, and in an extreme case, Fig. 5c, lead to a small reversed transpiration force.

Fig. 5b shows that for the case of Fig. 2f where an inverted velocity at the wall is observed, the momentum transfer–and thus the transpiration force–still has the same direction as for the fully diffusive surface, but it is much weaker. Blow-ups of the total momentum exchange are inserted in Fig. 5 for a detailed comparison. Hence, we must conclude that in this case the inverted tangential velocity at the wall *cannot* be attributed to the inversion of the transpiration force, but most likely results from a much weaker transpiration force at the boundary, which subsequently leads to domination of thermal stresses in the bulk.

In the original paper [10], the tangential velocity on the boundary is obtained utilizing the first order Chapman–Enskog expansion. Using Bird's notation for the shear stress [1], the tangential velocity was written as

$$\frac{\mathcal{V}_t}{\sqrt{\frac{k}{m}T_W}} = \frac{2-\chi}{\chi}\sqrt{\frac{\pi}{2}}\frac{\sigma_{nt}}{p} - \frac{\omega}{5}\frac{q_t}{p\sqrt{\frac{k}{m}T_W}}. \tag{9}$$

Here, $\mathcal{V}_t$ is the tangential velocity at the boundary, χ is the momentum accommodation coefficient, p is the pressure and ω is the coefficient for the strength of the thermal transpiration effect. We can see that the interplay between the shear stress σ_{nt} and the tangential heat flux, q_t determines the direction of the tangential velocity close to the surface. Choosing an appropriate set of α and γ in the VDM boundary condition enables us to reduce the influence of thermal transpiration, so that the shear stress dominates in determining the direction of the flow.

The shear stress, in the presence of small velocity and rather large thermal gradient in the flow field, is mainly influenced by the thermal stresses. Using the Grad equations [20] the shear stress in the bulk can be approximated as

$$\sigma_{tn} = \sigma_{tn}^{(1)} + \sigma_{tn}^{(2)}, \tag{10}$$

where the superscript shows the order in Knudsen number. Following Grad equations for the Maxwell molecule, and linearizing the shear stress in moments (small Knudsen number), we can write

$$\begin{aligned} \sigma_{tn}^{(1)} &= 2\mu\frac{\partial V_{<t}}{\partial x_{n>}}, \\ \sigma_{tn}^{(2)} &= \frac{4}{5}\frac{\mu}{p}\frac{\partial q_{<t}}{\partial x_{n>}}. \end{aligned} \tag{11}$$

Grad description for the shear stress shows that the thermal stresses are one order in Knudsen number higher than the viscous stresses. This means that thermal stresses will become important when the rarefaction is large (high Knudsen number regime); or when we are dealing with a flow at low velocity gradient and rather large heat flux gradient.

In order to confirm the role of thermal stresses in our thermal cavity flow, we used the DSMC result to obtain the shear stress in the first and second order, Eq. (11), along the horizontal centerline of the cavity. Fig. 6 shows the total stress, σ_{xy} as well as the viscous $\sigma_{xy}^{(1)}$ and thermal stresses $\sigma_{xy}^{(2)}$ for two choices of boundary condition coefficients. The solid line indicates the variation of the total stress in the horizontal centerline of the cavity. Note that

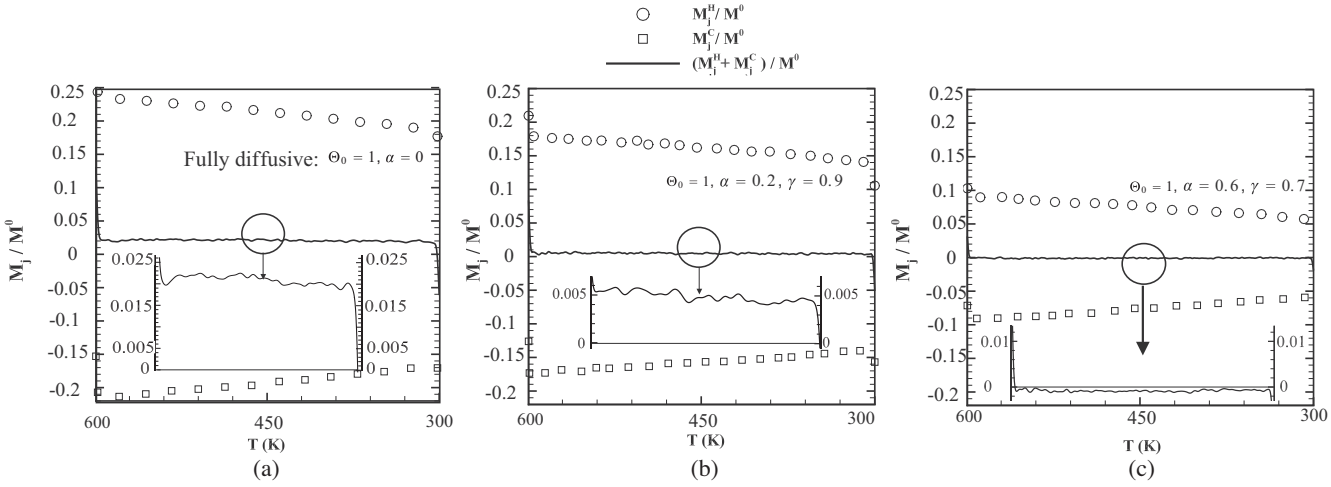

Fig. 5. Variation of the tangential momentum exchange on particle–surface level along the right wall for $Kn = 0.1$, $\varepsilon = 0$ and $\Theta_0 = 1$.

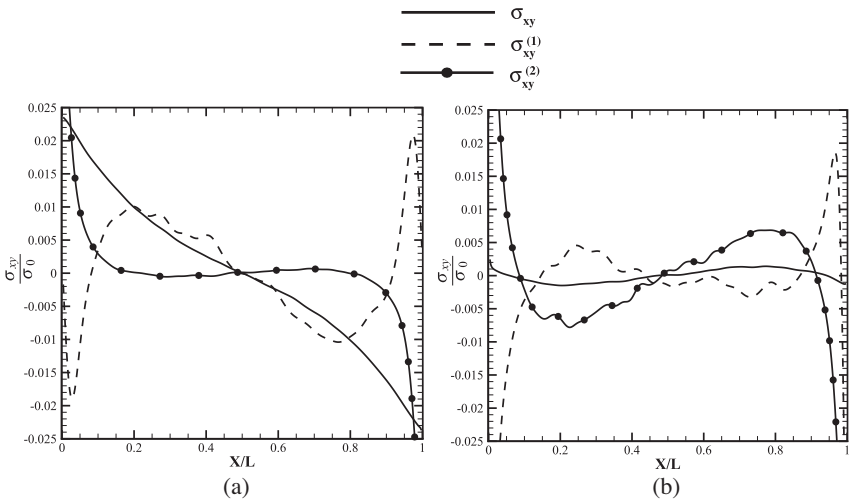

Fig. 6. Variation of shear stress component along the horizontal centerline of the cavity, (a) Fully diffusive surface: $\alpha = 0,\ \Theta_0 = 1$ (b) $\Theta_0 = 1\ \alpha = 0.2\ \gamma = 0.9$.

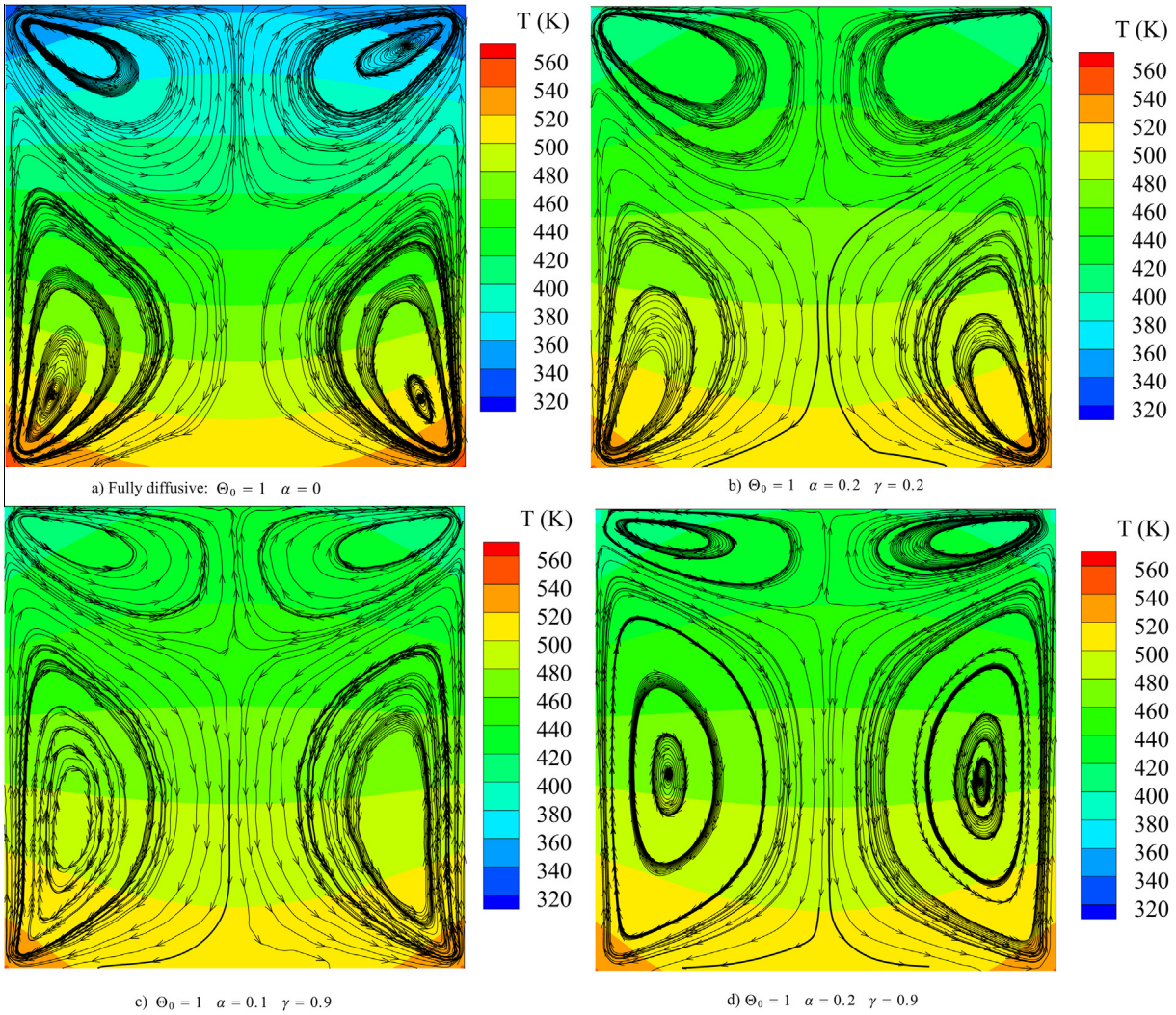

Fig. 7. Temperature distribution overlaid on the velocity streamlines at $Kn = 1$ and $\varepsilon = 0$.

the description of the shear stress in Eq. (10) is only valid in the bulk of the flow. When dealing with the Knudsen layer (in the vicinity of the walls) higher order moments can play a role and dominate in determining the shear stress.

For the fully diffusive surface, Fig. 6a the shear stress starts from a positive value close to the left wall and becomes negative as we pass the center of the cavity. The flow in this case is mainly driven by the boundaries, i.e., thermal transpiration. The tangential

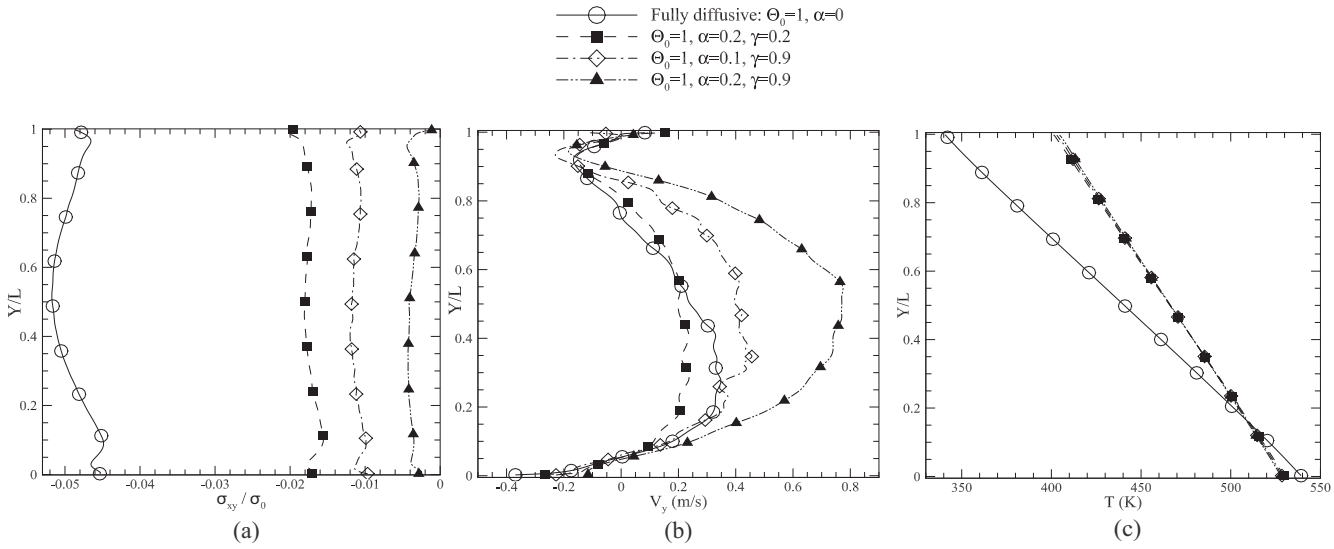

Fig. 8. The effect of α and γ on the flow properties along $\frac{X}{L} = 0.95$ for $Kn = 1,\ \varepsilon = 0$.

transpiration force accelerates the flow in the vicinity of the surface, which subsequently leads to appearance of the largest value of the shear stress at the wall. For the fully diffusive surface the total shear stress, σ_{xy} follows the trend of first order viscous stress $\sigma_{xy}^{(1)}$ in the bulk of the flow, i.e., outside of the Knudsen layer $\left(\frac{X}{L} \in [0.2, 0.8]\right)$. A quick look at Fig. 3b shows that the rarefied flow gets to its maximum velocity for the case of fully diffusive surface, and slows down for the VDM boundary conditions. This means that the viscous stress can take over the thermal stress, and dominate in determining the total stress for the fully diffusive surface. Fig. 6a also shows that the value of thermal stress in this case is very small, and rather close to zero in the main bulk of the flow. In this case it is safe to say that the thermal stresses do not play a big role in determining the shear stress. The imposed disturbance from the boundaries, coming from the thermal transpiration, is damped via the viscous stresses.

In the second case, Fig. 6b the total shear stress profile is different than what we observed for the fully diffusive surface, and changes sign multiple times along the horizontal centerline. Interestingly, the shear stress is one order of magnitude smaller in this case. Keeping in mind that the main source of disturbance in the flow field is the temperature gradient on the wall, the VDM boundary condition permits rather large number of particles to reflect back to the bulk without being influenced by the surface, i.e., specular reflection. In addition, the shear stress *does not* follow the trend of the velocity gradient, but rather has the same trend as the thermal stresses. Small values of the velocity, compared to the rather large values of the temperature gradient, in the flow field leads to domination of the thermal stresses in determining the total shear stress. This figure confirms the role of the thermal stresses in the secondary vortices appears in Fig. 2e.

It is also interesting to note that the very small values of the shear stress (close to zero) in this case implies that there is a balance between the thermal stresses and the viscous stress, $\sigma_{tn}^{(1)} = -\sigma_{tn}^{(2)}$. In a way, existence of rather large thermal gradient in the flow field drives the flow, and as a reaction, the viscous stresses damp the rarefied flow movement.

Above, we used the equations that are only valid for evaluating the bulk of the flow. As said above, we believe that in the cases of Fig. 2e and f the main driving force for the flow pattern are thermal stresses in the bulk–the secondary vortices most likely appear to bridge between the temperature driven bulk flow, and the boundaries.

4.4. Effect of Knudsen number

Following the discussion about the interplay between the first and second order of shear stress, and the capability of the VDM boundary conditions to manipulate their strength, we studied the effect of Knudsen number on the flow formation in the thermal cavity. To have a comparable set, we chose $Kn = 1$ and consider the same values of α and γ as in Section 4.2. Figure 7 shows the temperature distribution overlaid on the velocity streamlines inside the cavity. As was expected, rarefied flow experiences rather smaller temperature gradients in higher Knudsen regime, which is attributed to the larger temperature jump at this Knudsen number.

More interestingly, the vortex formation is different from what we observed at $Kn = 0.1$. Even for the fully diffusive surface, the secondary vortex in the vicinity of the side walls appears, and drives the flow from warm-to-cold. At this Knudsen number the Knudsen layer covers the entire cavity, and large rarefaction effects inside the domain leads to a large secondary vortex in the flow field. As we increase α the primary vortex, corresponding to the thermal transpiration, decreases in size and get pushed to the top corners of the cavity.

Fig. 8 shows the flow properties in the vicinity of the right wall along $\frac{X}{L} = 0.95$. It is seen that the vertical velocity close to the wall is changing sign for all choices of α and γ, which is in accordance with the appearance of primary and secondary vortices in Fig. 7. More interestingly, the larger positive value of the vertical velocity, i.e., warm-to-cold flow at $Kn = 1$ implies the rarefaction nature of the secondary vortex. The temperature profile close to the surface remains unchanged with respect to the corresponding coefficients in the VDM boundary conditions.

5. Conclusions

Velocity dependent Maxwell (VDM) boundary conditions are used in DSMC method to study the thermal transpiration effect. The flow formation inside a micro-cavity with the temperature gradient on the surface is studied. Thermal transpiration phenomena drives the rarefied flow from colder region toward the warmer

region for the fully diffusive surface. However, as the reflection kernel becomes dependent on the velocity of colliding particle to the surface, thermal transpiration becomes smaller in value. Particles with larger velocity (coming from the warm region) reflect back to the flow without being thermalized with the surface, while the slower particle (coming from the colder region) thermalize with the surface. As a result, using the VDM boundary condition, we can decrease/increase the strength of the thermal transpiration effect. This argument theoretically suggest the possibility of appearance of reversed thermal transpiration effect which drives the rarefied flow from warmer toward colder region. We observed the appearance of warm-to-cold vortices for certain choices of corresponding coefficients in the VDM boundary condition, and used DSMC to investigate their nature. Our study attributes the emerging warm-to-cold vortices to the thermal stresses in the bulk of the flow. In fact, the VDM boundary condition weakens the thermal transpiration effect, and subsequently permits the thermal stresses to dominate in determining the direction of the rarefied flow.

In classical hydrodynamics, transpiration flow is described by incorporating the wall temperature gradient as a driving force into the slip boundary condition. The DSMC simulations in the current study, show the inverted flow direction only at the boundary, while large vortices appear in the bulk. This flow behavior, most likely, is due to thermal stresses in the bulk, which cannot be described in classical hydrodynamics. Therefore, kinetic theory methods, like DSMC, direct numerical simulation [21], or advanced moment methods [22] must be used for the description, and understanding, of these flows. The VDM model is flexible, and can be incorporated in any of these advanced methods.

We note the lack of reliable experimental data that would be needed to fit the coefficients of the model.

Conflict of interest

None declared.

Acknowledgement

The authors would like to sincerely thank Professor Stefan Stefanov and Ehsan Roohi for their fruitful comments on this work. This research was supported by the Natural Sciences and Engineering Council (NSERC).

References

[1] G.A. Bird, Molecular Gas Dynamics and the Direct Simulation of Gas Flows, Oxford University Press, Oxford, 1994.
[2] E. Meiburg, Comparison of the molecular dynamics method and the direct simulation technique for flows around simple geometries, Phys. Fluids 29 (1986) 3107–3113.
[3] C. Cercignani, Theory and Application of the Boltzmann Equation, Scottish academic press, Edinburgh, 1975.
[4] J.J. Hinchen, W. Foley, Scattering of molecular beams by metallic surfaces, Proceedings of the Fourth International Symposium.
[5] C. Cercignani, M. Lampis, Kinetic models for gas–surface interactions, Transp. Theory Stat. Phys. 1 (1971) 101–114.
[6] R.G. Lord, Some extensions to the Cercignani–Lampis gas–surface scattering kernel, Phys. Fluids A 3 (1991) 706–710.
[7] F. Sharipov, Application of the Cercignani–Lampis scattering kernel to calculations of rarefied gas flows. II. Slip and jump coefficients, Eur. J. Mech. B/Fluids 22 (2003) 133–143.
[8] J.C. Maxwell, On stresses in rarified gases arising from inequalities of temperature, Philos. Trans. R. Soc. Lond. 170 (1879) 231–256.
[9] M. Epstein, Predicting continuum breakdown of rarefied micro/nano flows using entropy and entropy generation analysis, AIAA J. 5 (1967) 1797.
[10] H. Struchtrup, Maxwell boundary condition and velocity dependent accommodation coefficient, Phys. Fluids 25 (2013) 112001.
[11] A. Mohammadzadeh, A.S. Rana, H. Struchtrup, Viscous slip heating: DSMC and R13 modeling of the adiabatic surface, Submitted.
[12] A.S. Rana, A. Mohammadzadeh, H. Struchtrup, A numerical study of the heat transfer through a rarefied gas confined in a micro cavity, Accepted for publication in Cont. Mech. Thermodyn.
[13] M. Vargas, G. Tatsios, D. Valougeorgis, Rarefied gas flow in a rectangular enclosure induced by non-isothermal walls, Phys. Fluid 26 (2014) 057101.
[14] C. Cai, Heat transfer in vacuum packaged micro-electro-mechanical system devices, Phys. Fluid 20 (2008) 017103.
[15] Y. Sone, Comment on heat transfer in vacuum packaged micro-electro-mechanical system devices. Phys. Fluids 20 (2008) 017103. Phys. Fluid 21 (2009) 119101.
[16] S. Kosuge, K. Aoki, S. Takata, R. Hattori, D. Sakai, Steady flows of a highly rarefied gas induced by nonuniform wall temperature, Phys. Fluid 23 (2011) 030603.
[17] A. Mohammadzadeh, E. Roohi, H. Niazmand, S. Stefanov, R. Myong, Thermal and second-law analysis of a micro- or nano-cavity using direct-simulation Monte Carlo, Phys. Rev. E 85 (2012) 056310.
[18] A. Mohammadzadeh, E. Roohi, H. Niazmand, A parallel DSMC investigation of monatomic/diatomic gas flow in micro/nano cavity, Numer. Heat Tr. A 63.
[19] H. Niazmand, A. Mohammadzadeh, E. Roohi, Predicting continuum breakdown of rarefied micro/nano flows using entropy and entropy generation analysis, Int. J. Mod. Phys. C 24 (2013) 1350029–1350039.
[20] H. Struchtrup, Macroscopic Transport Equations for Rarefied Gas Flows, Springer, Berlin, 2005.
[21] T. Ohwada, Y. Sone, K. Aoki, Numerical analysis of the Poiseuille and thermal transpiration flows between two parallel plates on the basis of the Boltzmann equation for hardsphere molecules, Phys. Fluids A 1 (1989) 2042.
[22] P. Taheri, H. Struchtrup, Rarefaction effects in thermally-driven microflows, Phys. A 389 (2010) 3069–3089.